`dftatom`: A robust and general Schrödinger and Dirac solver for atomic structure calculations

Ondřej Čertík [a,b,c], John E. Pask [d], Jiří Vackář [a]

[a] *Institute of Physics, Academy of Sciences of the Czech Republic, Na Slovance 2, 182 21 Praha 8, Czech Republic*

[b] *University of Nevada, Reno - 1664 N. Virginia St., Reno, NV 89557-0208, USA*

[c] *Faculty of Mathematics and Physics, Charles University, Ke Karlovu 3, 121 16 Praha 2, Czech Republic*

[d] *Lawrence Livermore National Laboratory, 7000 East Avenue, Livermore, CA 94550, USA*

Abstract

A robust and general solver for the radial Schrödinger, Dirac, and Kohn–Sham equations is presented. The formulation admits general potentials and meshes: uniform, exponential, or other defined by nodal distribution and derivative functions. For a given mesh type, convergence can be controlled systematically by increasing the number of grid points. Radial integrations are carried out using a combination of asymptotic forms, Runge-Kutta, and implicit Adams methods. Eigenfunctions are determined by a combination of bisection and perturbation methods for robustness and speed. A novel outward Poisson integration is employed to increase accuracy in the core region, allowing absolute accuracies of 10^{-8} Hartree to be attained for total energies of heavy atoms such as uranium. Detailed convergence studies are presented and computational parameters are provided to achieve accuracies commonly required in practice. Comparisons to analytic and current-benchmark density-functional results for atomic number $Z = 1$–92 are presented, verifying and providing a refinement to current benchmarks. An efficient, modular Fortran 95 implementation, `dftatom`, is provided as open source, including examples, tests, and wrappers for interface to other languages; wherein particular emphasis is placed on the independence (no global variables), reusability, and generality of the individual routines.

Key words: atomic structure, electronic structure, Schrödinger equation, Dirac equation, Kohn–Sham equations, density functional theory, shooting method, Fortran 95, Python, C
PACS:

PROGRAM SUMMARY

Manuscript Title: `dftatom`: A robust and general Schrödinger and Dirac solver for atomic structure calulations
Authors: Ondřej Čertík, John E. Pask, Jiří Vackář
Program Title: dftatom
Journal Reference:
Catalogue identifier:
Licensing provisions: MIT license
Programming language: Fortran 95 with interfaces to Python and C
Computer: Any computer with Fortran 95 compiler
Operating system: Any OS with Fortran 95 compiler
RAM: 500 MB
Number of processors used:
Keywords:
atomic structure, electronic structure, Schrödinger equation, Dirac equation, Kohn–Sham equations, density functional theory, shooting method, Fortran 95, Python, C
Classification: 2.1 Structure and Properties
Nature of problem:
Solution of the Schrödinger, Dirac, and Kohn–Sham equations of Density Functional Theory for isolated atoms.
Solution method:
Radial integrations are carried out using a combination of asymptotic forms, Runge-Kutta, and implicit Adams methods. Eigenfunctions are determined by a combination of bisection and perturbation methods. An outward Poisson integration is employed to increase accuracy in the core region. Self-consistent field equations are solved by adaptive linear mixing.
Restrictions: Spherical symmetry
Unusual features:
Radial integrators work for general potentials and meshes. No restriction to Coulombic or self-consistent potentials; no restriction to uniform or exponential meshes. Outward Poisson integration. Fallback to bisection for robustness.
Additional comments:
Running time: For uranium, non-relativistic density functional calculation execution time is around 0.6s for 10^{-6} a.u. accuracy in total energy on Intel Core i7 1.46GHz processor.

Email addresses: `ondrej.certik@gmail.com` (Ondřej Čertík), `pask1@llnl.gov` (John E. Pask), `vackar@fzu.cz` (Jiří Vackář).

1 Introduction

Atomic structure calculations are a lynchpin of modern materials theory. They provide the basis for understanding the properties of individual atoms and play a central role in electronic structure calculations of larger, multi-atom systems such as molecules, nanostructures, and solids [1]. In the latter context, being a core computational kernel for larger-scale calculations, both accuracy and efficiency are of prime importance. Such atomic calculations, solving radial Schrödinger or Dirac equations, can be found at the heart of plasma physics calculations [2], all-electron electronic structure methods such as Korringa–Kohn–Rostoker (KKR) [3], linearized muffin tin orbital (LMTO) [4], and linearized augmented planewave (LAPW) [5], pseudo-atomic-orbital based methods [6], *ab initio* pseudopotential construction [1], and projector augmented wave (PAW) [7], relaxed-core PAW [8], and all-electron pseudopotential (AEPP) [9] methods, among others.

Due to their central importance in the full range of electronic structure calculations, from isolated atoms to solids, a number of atomic structure codes have been developed over the decades, see, e.g., [10–15]. However, most have been developed within, and remain closely tied to, the specific larger-scale method of which they are a part, and hence are difficult to separate and use for other purposes. Indeed, it was precisely our own need for a robust and general solver for use in a finite-element [16] based AEPP [9] method that motivated the present work. Beyond difficulty to extract, however, existing codes have widely differing capabilities, efficiencies, robustness, and availability. Table 1 lists features of several established codes. Some solve the equations of density functional theory (DFT) while others solve Hartree-Fock (HF). Some are relativistic, others not. Some can be converged to high precision while others can be difficult to converge beyond the accuracies required by the larger codes of which they are a part. Some allow any mesh while others implement only exponential meshes. Some allow any potential while others implement only singular all-electron potentials. Some implement perturbation corrections for speed, others only bisection. Some are open source, others not. Note that the table shows only shooting-type solvers [17], as we discuss in the present work. Other non-shooting type approaches (see, e.g., [18,19] and references therein) have been developed and implemented as well but have not yet found wide adoption in larger-scale electronic structure calculations due in part to robustness issues (e.g., spurious states) which can arise [19]. Note also that the table is intended only as a general guide: in the context of any given feature, "No" should be understood to mean only that we did not find it straightforward to implement in the referenced code.

In the present work, we bring together ideas from a host of atomic structure codes developed over many decades, and add new ideas to increase ac-

Code	dftatom	Desclaux	atompp	grasp2k	atompaw	PEtot	Elk
Reference	This work	[10]	[11]	[12]	[13]	[14]	[15]
Open Source	MIT	No	No	No	GPL	BSD	GPL
Schrödinger	Yes	No	Yes	No	Yes	Yes	No
Dirac	Yes	Yes	No	Yes	No	Yes	Yes
DFT	Yes	No	Yes	No	Yes	Yes	Yes
Any potential	Yes	No	Yes	No	No	No	Yes
Any mesh	Yes	No	No	No	No	No	Yes
Outward Poisson	Yes	No	No	No	No	No	No
Perturb. correct.	Yes	Yes	Yes	No	Yes	Yes	No
Bisection fallback	Yes	No	No	No	No	No	No

Table 1
Features of various atomic structure solvers.

curacy and robustness. We try to do this in such a way as to provide as general, flexible, and efficient a tool as possible, facilitating subsequent use in a range of applications areas. We develop and implement solvers for the radial Schrödinger, Dirac, and Kohn–Sham equations. The formulation allows general potentials and meshes: singular Coulomb-, finite pseudo-, or other potentials; uniform, exponential, or other meshes, as defined by nodal distributions and derivatives. For a given mesh type, convergence can be controlled systematically by increasing the number of grid points. Radial integrations are carried out using a combination of asymptotic forms, Runge-Kutta, and implicit Adams methods. Eigenfunctions are determined by a combination of bisection and perturbation methods for robustness and speed. We employ a novel outward Poisson integration to increase accuracy in the core region, allowing absolute accuracies of 10^{-8} Hartree to be attained for total energies of heavy atoms such as uranium. We show detailed convergence studies and provide computational parameters to achieve accuracies commonly required in practice. We present comparisons to analytic and current-benchmark density-functional results [20,21] for atomic number $Z = 1$–92, verifying and refining current benchmarks.

We provide an efficient, modular Fortran 95 implementation, `dftatom`, as open source, including examples, tests, and wrappers for interface to other languages. The code consists of several clearly arranged Fortran 95 modules, designed to be easy to apply for other purposes. The integration routines are independent of mesh, which can be specified as desired. Routines for common meshes are provided. Extensive tests are included to verify the correctness of results and serve as examples for a number of cases: Coulombic, self consistent DFT, and non-singular potentials; exponential and hyperbolic meshes; atomic numbers $Z = 1$–92; user-specified occupation numbers; and others. The code is opensource, available under the terms of the MIT license, from [22]. C and Python wrappers are provided so that the code can be easily used from other languages as well as interactively from Python.

The remainder of the paper is organized as follows. Section 2 describes the radial Schrödinger, Dirac, and Poisson equations, associated asymptotics, and DFT equations to be solved. Section 3 describes the numerical methods used to solve the radial equations and eigenproblem, and meshes employed. Section 4 shows Schrödinger and Dirac results for a Coulombic potential and harmonic oscillator potential, relativistic and nonrelativistic DFT calculations of uranium, convergence studies determining parameters for specified accuracies, and comparison to established benchmarks [20]. We conclude in Section 5.

2 Equations

2.1 Radial Schrödinger equation

The 3D one-electron Schrödinger equation is given by

$$\left(-\tfrac{1}{2}\nabla^2 + V(\mathbf{x})\right)\psi(\mathbf{x}) = E\psi(\mathbf{x}), \tag{1}$$

in Hartree atomic units, as we use throughout. For a spherically symmetric potential

$$V(\mathbf{x}) = V(r), \tag{2}$$

eigenstates of energy and angular momentum can be written in the form

$$\psi_{nlm}(\mathbf{x}) = R_{nl}(r)\, Y_{lm}\left(\frac{\mathbf{x}}{r}\right), \tag{3}$$

where n is the principle quantum number, l is the orbital angular momentum quantum number, and m is the magnetic quantum number; whereupon it follows that $R_{nl}(r)$ satisfies the radial Schrödinger equation

$$\left(-\tfrac{1}{2}r^2 R'_{nl}(r)\right)' + \left(r^2 V + \tfrac{1}{2}l(l+1)\right) R_{nl}(r) = Er^2 R_{nl}(r). \tag{4}$$

The functions $\psi_{nlm}(\mathbf{x})$ and $R_{nl}(r)$ are normalized as

$$\int |\psi_{nlm}(\mathbf{x})|^2 \,\mathrm{d}^3x = 1, \tag{5}$$

$$\int_0^\infty R_{nl}^2(r) r^2 \,\mathrm{d}r = 1. \tag{6}$$

The substitution $P_{nl}(r) = rR_{nl}(r)$ and $Q_{nl}(r) = P'_{nl}(r) = R_{nl}(r) + rR'_{nl}(r)$ can be used to write the second-order radial Schrödinger equation as a coupled set of first-order equations:

$$P'_{nl}(r) = Q_{nl}(r), \tag{7}$$

$$Q'_{nl}(r) = 2\left(V(r) - E + \frac{l(l+1)}{2r^2}\right) P_{nl}(r). \tag{8}$$

Such a first-order formulation facilitates solving both nonrelativistic Schrödinger and relativistic Dirac equations using the same techniques. The normalization of $P(r)$ is

$$\int_0^\infty P_{nl}^2(r)\,\mathrm{d}r = 1. \tag{9}$$

For a potential $V(r)$ which behaves like $-Z/r + V_0$ near the origin, as in the vicinity of the nucleus, the asymptotic behaviors of P_{nl} and Q_{nl} are [23]

$$P_{nl}(r) = r^{l+1}, \tag{10}$$
$$Q_{nl}(r) = (l+1)r^l. \tag{11}$$

For large r, assuming $V(r) \to 0$ as $r \to \infty$, the asymptotic is [23]:

$$P_{nl}(r) = e^{-\lambda r}, \tag{12}$$
$$Q_{nl}(r) = -\lambda P_{nl}(r), \tag{13}$$

where

$$\lambda = \sqrt{-2E_{nl}}\,. \tag{14}$$

As solutions of a homogeneous system, P_{nl} and Q_{nl} are unique only up to an arbitrary multiplicative constant. These small- and large-r asymptotics provide starting values and derivatives for inward and outward numerical integrations.

2.2 Radial Dirac equation

The one-electron radial Dirac equation can be written as

$$P'(r) = -\frac{\kappa}{r}P(r) + \left(\frac{E - V(r)}{c} + 2c\right)Q(r), \tag{15}$$
$$Q'(r) = -\left(\frac{E - V(r)}{c}\right)P(r) + \frac{\kappa}{r}Q(r), \tag{16}$$

where $P(r)$ and $Q(r)$ are related to the usual large $g(r)$ and small $f(r)$ components of the Dirac equation by

$$P(r) = rg(r), \tag{17}$$
$$Q(r) = rf(r). \tag{18}$$

See for example [24,25] for a discussion and derivation. The energy E does not contain the electron rest mass energy, so it can be compared directly to the corresponding nonrelativistic energy of the Schrödinger equation. The normalization of $P(r)$ and $Q(r)$ is

$$\int_0^\infty (P^2(r) + Q^2(r))\,\mathrm{d}r = 1. \tag{19}$$

For potentials of the form $V(r) = -Z/r + Z_1 + O(r)$, the asymptotic behavior at the origin for $Z \neq 0$ (Coulombic) is [26,25]

$$P(r) = r^\beta, \tag{20}$$

$$Q(r) = r^\beta \frac{c(\beta + \kappa)}{Z}, \tag{21}$$

where

$$\beta = \sqrt{\kappa^2 - \left(\frac{Z}{c}\right)^2}. \tag{22}$$

For $Z = 0$ (nonsingular) the asymptotic is [26], for $\kappa < 0$

$$P(r) = r^{l+1}, \tag{23}$$

$$Q(r) = r^{l+2} \frac{E + Z_1}{c(2l+3)}, \tag{24}$$

and for $\kappa > 0$

$$P(r) = -r^{l+2} \frac{E + Z_1}{c(2l+1)}, \tag{25}$$

$$Q(r) = r^{l+1}. \tag{26}$$

For large r, assuming $V(r) \to 0$ as $r \to \infty$, the asymptotic is [23]

$$P(r) = e^{-\lambda r}, \tag{27}$$

$$Q(r) = -\sqrt{-\frac{E}{E + 2c^2}} P(r), \tag{28}$$

$$\tag{29}$$

where

$$\lambda = \sqrt{c^2 - \frac{(E + c^2)^2}{c^2}} = \sqrt{-2E - \frac{E^2}{c^2}}. \tag{30}$$

As in the case of the Schrödinger equation, $P_{n\kappa}$ and $Q_{n\kappa}$ are unique only up to an arbitrary multiplicative constant, and the above asymptotics provide starting values and derivatives for inward and outward numerical integrations.

The solutions of the Dirac equation are labeled by quantum numbers n and κ, where $\kappa \neq 0$ is an integer. Alternatively, they may be labeled by the triplet n, l, s, where $s = \pm 1$ distinguishes $j = l \pm \frac{1}{2}$ states. κ is then determined by

$$\kappa = \begin{cases} -l - 1 & \text{for } j = l + \frac{1}{2} \ (s = +1), \\ l & \text{for } j = l - \frac{1}{2} \ (s = -1). \end{cases} \tag{31}$$

2.3 Poisson equation

The 3D Poisson equation for the Hartree potential V_H due to electronic density n is given by

$$\nabla^2 V_H(\mathbf{x}) = -4\pi n(\mathbf{x}). \tag{32}$$

For a spherical density $n(\mathbf{x}) = n(r)$, this becomes

$$\frac{1}{r^2}(r^2 V_H')' = V_H''(r) + \frac{2}{r}V_H'(r) = -4\pi n(r), \tag{33}$$

where $n(r)$ is the radial particle (number) density, normalized such that

$$Z = \int n(\mathbf{x})\,\mathrm{d}^3x = \int_0^\infty 4\pi n(r) r^2\,\mathrm{d}r. \tag{34}$$

Substituting (33) into (34) and integrating, we obtain

$$\lim_{r\to\infty} r^2 V_H'(r) = -Z, \tag{35}$$

from which it follows that the asymptotic behavior of $V_H'(r)$ is

$$V_H'(r) = -\frac{Z}{r^2}, \qquad r \to \infty. \tag{36}$$

Integrating (36) and requiring $V_H \to 0$ as $r \to \infty$ then gives the corresponding asymptotic behavior for $V_H(r)$:

$$V_H(r) = \frac{Z}{r}, \qquad r \to \infty. \tag{37}$$

For small r, the asymptotic behavior can be obtained by expanding $n(r)$ about $r = 0$: $n(r) = \sum_{j=0}^\infty c_j r^j$. Substituting into Poisson equation (33) gives

$$(r^2 V_H')' = -4\pi \sum_{j=0}^\infty c_j r^{j+2}. \tag{38}$$

Integrating and requiring $V_H(0)$ finite then gives

$$V_H'(r) = -4\pi \sum_{j=0}^\infty c_j \frac{r^{j+1}}{j+3}, \tag{39}$$

with linear leading term; so that we have

$$V_H'(r) \propto r, \qquad r \to 0. \tag{40}$$

Integrating (39) then gives

$$V_H(r) = -4\pi \sum_{j=0}^\infty c_j \frac{r^{j+2}}{(j+2)(j+3)} + C, \tag{41}$$

with leading constant term $C = V_H(0)$ determined by Coulomb's law:

$$V_H(0) = 4\pi \int_0^\infty r n(r)\,\mathrm{d}r. \tag{42}$$

Finally, from (40) we have that

$$V_H'(0) = 0. \tag{43}$$

The above asymptotics provide starting values and derivatives for inward and outward numerical integrations.

2.4 Kohn–Sham equations

The Kohn–Sham equations consist of the radial Schrödinger or Dirac equations above with an effective potential $V(r) = V_{\mathrm{in}}(r)$ given by (see, e.g., [1])

$$V_{\mathrm{in}} = V_H + V_{xc} + v, \tag{44}$$

where V_H is the Hartree potential given by the solution of the radial Poisson equation (33), V_{xc} is the exchange-correlation potential and $v = -\frac{Z}{r}$ is the nuclear potential.

The total energy is given by

$$E[n] = T_s[n] + E_H[n] + E_{xc}[n] + V[n], \tag{45}$$

the sum of kinetic energy

$$T_s[n] = \sum_{nl} f_{nl}\epsilon_{nl} - 4\pi \int V_{\mathrm{in}}(r) n(r) r^2\,\mathrm{d}r, \tag{46}$$

Hartree energy

$$E_H[n] = 2\pi \int V_H(r) n(r) r^2\,\mathrm{d}r, \tag{47}$$

exchange-correlation energy

$$E_{xc}[n] = 4\pi \int \epsilon_{xc}(r; n) n(r) r^2\,\mathrm{d}r, \tag{48}$$

and Coulomb energy

$$V[n] = 4\pi \int v(r) n(r) r^2\,\mathrm{d}r = -4\pi Z \int n(r) r\,\mathrm{d}r; \tag{49}$$

with electronic density in the nonrelativistic case given by

$$n(r) = \frac{1}{4\pi} \sum_{nl} f_{nl} \frac{P_{nl}^2(r)}{r^2}, \tag{50}$$

where P_{nl} is the radial wavefunction (Eq. (7)) and f_{nl} the associated electronic occupation. In the relativistic case, the electronic density is given by

$$n(r) = \frac{1}{4\pi} \sum_{nls} f_{nls} \frac{P_{nls}^2(r) + Q_{nls}^2(r)}{r^2}, \tag{51}$$

where P_{nls} and Q_{nls} are the two components of the Dirac solution (Eqs. (15), (16)) and f_{nls} is the occupation. In both cases above, $n(r)$ is the electronic particle density [electrons/volume], everywhere positive, as distinct from the electronic charge density $\rho(r)$ [charge/volume]: $\rho(r) = -n(r)$ in atomic units.

These equations are solved self-consistently (see, e.g., [1]): an initial density n_{in} and corresponding potential V_{in} are constructed; the Schrödinger or Dirac equation is solved to determine wavefunctions R_{nl} or spinor components P and Q, respectively; from these a new density n_{out} and potential V_{out} are constructed; and from these, a new input density n_{in} and potential V_{in} are constructed. The process is continued until the difference of V_{in} and V_{out} and/or n_{in} and n_{out} is within a specified tolerance, at which point *self-consistency* is achieved. This fixed point iteration is known as the *self-consistent field* (SCF) iteration. We employ an adaptive linear mixing scheme, with optimized weights for each component of the potential to construct new input potentials for successive SCF iterations. In order to reduce the number of SCF iterations, we use a Thomas-Fermi (TF) approximation [27] for the initial density and potential:

$$V(r) = -\frac{Z_{\text{eff}}(r)}{r}, \tag{52}$$

where

$$Z_{\text{eff}}(r) = Z(1 + \alpha\sqrt{x} + \beta x e^{-\gamma\sqrt{x}})^2 e^{-2\alpha\sqrt{x}}, \tag{53}$$

$$x = r\left(\frac{128Z}{9\pi^2}\right)^{\frac{1}{3}}, \tag{54}$$

$$\alpha = 0.7280642371, \tag{55}$$

$$\beta = -0.5430794693, \tag{56}$$

$$\gamma = 0.3612163121. \tag{57}$$

The corresponding charge density is then

$$\rho(r) = -\frac{1}{3\pi^2}\left(-2V(r)\right)^{\frac{3}{2}}. \tag{58}$$

For simplicity, we consider only local-density approximation (LDA) and relativistic local-density approximation (RLDA) exchange and correlation potentials here. More sophisticated functionals can be readily incorporated. Our `dftatom` implementation uses the same parameterization as in NIST benchmarks [20]:

$$V_{xc}(r; n) = \frac{\mathrm{d}}{\mathrm{d}n}\left(n\epsilon_{xc}^{LD}(n)\right), \tag{59}$$

where the exchange and correlation energy density ϵ_{xc}^{LD} can be written as [1]

$$\epsilon_{xc}^{LD}(n) = \epsilon_x^{LD}(n) + \epsilon_c^{LD}(n), \tag{60}$$

with electron gas exchange term [1]

$$\epsilon_x^{LD}(n) = -\frac{3}{4\pi}(3\pi^2 n)^{\frac{1}{3}} \tag{61}$$

and Vosko-Wilkes-Nussair (VWN) [28] correlation term

$$\epsilon_c^{LD}(n) \approx \frac{A}{2}\left\{\ln\left(\frac{y^2}{Y(y)}\right) + \frac{2b}{Q}\arctan\left(\frac{Q}{2y+b}\right) - \frac{by_0}{Y(y_0)}\left[\ln\left(\frac{(y-y_0)^2}{Y(y)}\right) + \frac{2(b+2y_0)}{Q}\arctan\left(\frac{Q}{2y+b}\right)\right]\right\}, \tag{62}$$

in which $y = \sqrt{r_s}$, $Y(y) = y^2 + by + c$, $Q = \sqrt{4c - b^2}$, $y_0 = -0.10498$, $b = 3.72744$, $c = 12.9352$, $A = 0.0621814$, and

$$r_s = \left(\frac{3}{4\pi n}\right)^{\frac{1}{3}} \tag{63}$$

is the Wigner-Seitz radius, which gives the mean distance between electrons. In the relativistic (RLDA) case, a correction to the LDA exchange energy density and potential is given by MacDonald and Vosko [29]:

$$\epsilon_x^{RLD}(n) = \epsilon_x^{LD}(n)R, \tag{64}$$

$$R = 1 - \frac{3}{2}\left(\frac{\beta\mu - \ln(\beta+\mu)}{\beta^2}\right)^2,$$

$$V_x^{RLD}(n) = V_x^{LD}(n)S, \tag{65}$$

$$S = \frac{3\log(\beta+\mu)}{2\beta\mu} - \tfrac{1}{2},$$

where $\mu = \sqrt{1+\beta^2}$ and $\beta = \frac{(3\pi^2 n)^{\frac{1}{3}}}{c} = -\frac{4\pi\epsilon_x^{LD}(n)}{3c}$.

3 Methods of solution

In this section, we discuss the radial integration methods, meshes, and eigenfunction isolation methods employed in the Kohn–Sham solution.

3.1 Runge-Kutta and Adams methods

To allow general, nonuniform meshes, all methods first transform equations on a general mesh $R(t)$, $1 \leq t \leq N+1$, to equations on a uniform mesh t with step size $h = 1$. If the solution on a general mesh is $P(r)$ and the transformed solution on the uniform mesh is $u(t)$ then

$$u(t) = P(R(t)) \tag{66}$$

$$u'(t) = \frac{\mathrm{d}u}{\mathrm{d}t} = \frac{\mathrm{d}P}{\mathrm{d}R} R'(t) \tag{67}$$

$$\tag{68}$$

The methods below require the values $u(t)$ and derivatives $u'(t)$ on the uniform mesh, which we express in terms of the values $P(r)$ and derivatives $P'(r)$ on the general mesh, and derivative $R'(t)$ of the function defining the general mesh.

The Runge-Kutta family of methods for the numerical integration of ordinary differential equations require the values of dependent and independent variables in the interior of the element (step). For example, the 4th-order Runge-Kutta (RK4) step for an equation of the form $y' = f(x, y)$ is:

$$y_{i+1} = y_i + \frac{1}{6}(k_1 + 2k_2 + 2k_3 + k_4), \tag{69}$$

$$k_1 = f(x_i, y_i), \tag{70}$$

$$k_2 = f(x_{i+\frac{1}{2}}, y_i + \tfrac{1}{2}k_1), \tag{71}$$

$$k_3 = f(x_{i+\frac{1}{2}}, y_i + \tfrac{1}{2}k_2), \tag{72}$$

$$k_4 = f(x_{i+1}, y_i + k_3). \tag{73}$$

Implicit Adams methods, on the other hand, use an extrapolation formula to advance the solution to the next grid point and then an interpolation formula to correct the value (predictor-corrector) using the grid points only. The 4th-order Adams outward extrapolation is given by

$$y_{i+1} = y_i + \frac{1}{24}(55y'_i - 59y'_{i-1} + 37y'_{i-2} - 9y'_{i-3}) \tag{74}$$

and interpolation by

$$y_{i+1} = y_i + \frac{1}{24}(9y'_{i+1} + 19y'_i - 5y'_{i-1} + y'_{i-2}). \tag{75}$$

Since the Schrödinger and Dirac equations are linear (for given effective potential in each SCF iteration), the interpolation can be determined analytically, thus eliminating predictor-corrector iterations, speeding up the calculation

considerably. Both Schrödinger and Dirac equations can be written as

$$\begin{pmatrix} P' \\ Q' \end{pmatrix} = C \begin{pmatrix} P \\ Q \end{pmatrix}, \tag{76}$$

where for the Schrödinger equation, the matrix C is given by

$$C(i) = \begin{pmatrix} 0 & 1 \\ \frac{l(l+1)}{R^2(i)} + 2(V(i) - E) & 0 \end{pmatrix} \tag{77}$$

and for the Dirac equation,

$$C(i) = \begin{pmatrix} -\frac{\kappa}{R(i)} & \frac{E-V(i)}{c} + 2c \\ -\frac{E-V(i)}{c} & \frac{\kappa}{R(i)} \end{pmatrix}. \tag{78}$$

Then for outward integration, analytic interpolation gives:

$$\lambda = \frac{9}{24}, \tag{79}$$

$$\Delta = 1 + \lambda^2 R'^2(i+1) \det C(i+1), \tag{80}$$

$$M = \frac{1}{\Delta}\left(\begin{pmatrix} 1 & 0 \\ 0 & 1 \end{pmatrix} + \lambda R'(i+1) \begin{pmatrix} -C_{22}(i+1) & C_{12}(i+1) \\ C_{21}(i+1) & -C_{11}(i+1) \end{pmatrix}\right), \tag{81}$$

$$\begin{pmatrix} u_1(i+1) \\ u_2(i+1) \end{pmatrix} = M \begin{pmatrix} u_1(i) + \frac{1}{24}(19u_1'(i) - 5u_1'(i-1) + u_1'(i-2)) \\ u_2(i) + \frac{1}{24}(19u_2'(i) - 5u_2'(i-1) + u_2'(i-2)) \end{pmatrix}. \tag{82}$$

See [23] for a detailed discussion.

For inward integration, the 4th order Adams inward extrapolation is given by

$$y_{i-1} = y_i - \frac{1}{24}(55y_i' - 59y_{i+1}' + 37y_{i+2}' - 9y_{i+3}') \tag{83}$$

and interpolation by

$$y_{i-1} = y_i - \frac{1}{24}(9y_{i-1}' + 19y_i' - 5y_{i+1}' + y_{i+2}'), \tag{84}$$

in which case, analytic interpolation gives:

$$\lambda = -\frac{9}{24}, \tag{85}$$

$$\Delta = 1 + \lambda^2 R'^2(i-1) \det C(i-1), \tag{86}$$

$$M = \frac{1}{\Delta}\left(\begin{pmatrix}1 & 0\\ 0 & 1\end{pmatrix} + \lambda R'(i-1)\begin{pmatrix}-C_{22}(i-1) & C_{12}(i-1)\\ C_{21}(i-1) & -C_{11}(i-1)\end{pmatrix}\right), \tag{87}$$

$$\begin{pmatrix}u_1(i-1)\\ u_2(i-1)\end{pmatrix} = M\begin{pmatrix}u_1(i) - \frac{1}{24}(19u_1'(i) - 5u_1'(i+1) + u_1'(i+2))\\ u_2(i) - \frac{1}{24}(19u_2'(i) - 5u_2'(i+1) + u_2'(i+2))\end{pmatrix}. \tag{88}$$

In practice, we use RK4 to compute the first 4 points needed by implicit Adams, then switch to the more accurate implicit Adams method to compute the remaining points.

3.2 Mesh

The methods discussed here can use any desired mesh: uniform, hyperbolic, exponential, or other. In practice, however, as we show below, most atomic structure codes use some form of exponential (or "logarithmic") mesh, as this gives an efficient concentration of mesh points in the vicinity of the Coulomb singularity, where wavefunctions, densities, and potentials vary most rapidly. Given their particular prevalence, we discuss exponential meshes below, and provide associated routines in the `dftatom` distribution.

Every exponential mesh can be written as a function of exactly four parameters, $r_{\min}$, $r_{\max}$, a, and N, as follows:

$$R_i = \alpha\left(e^{\beta(i-1)} - 1\right) + r_{\min}, \tag{89}$$

$$\alpha = \frac{r_{\max} - r_{\min}}{e^{\beta N} - 1}, \tag{90}$$

$$\beta = \frac{\log a}{N-1}. \tag{91}$$

for $i = 1, 2, \ldots, N+1$. Note that in the above we have explicitly included an arbitrary shift of origin. Without this, three parameters are of course sufficient to specify an exponential mesh. As we elaborate below, however, the flexibility to choose the initial point independent of other mesh parameters affords additional efficiency when employing asymptotic expressions for initial values. In the above form, all parameters have direct physical meaning: the mesh starts at $R_1 = r_{\min}$ and ends at $R_{N+1} = r_{\max}$; as shown below, the parameter a is the ratio of rightmost to leftmost element (mesh interval) lengths

(determining the mesh gradation), and N is the number of elements in the mesh. The ratio q of any two successive elements can be calculated from (89):

$$q = \frac{R_{n+1} - R_n}{R_n - R_{n-1}} = e^{\beta} = a^{\frac{1}{N-1}}. \tag{92}$$

It follows that the mesh gradation a can be expressed using the ratio q as $a = q^{N-1}$ and thus a is the ratio of rightmost to leftmost element lengths.

The main advantage of this parametrization is that $r_{\min}$ and $r_{\max}$ are decoupled from the mesh gradation and number of elements and can thus be varied independently. Once $r_{\min}$ is determined to provide sufficiently accurate asymptotic values, there is still freedom to change the gradation of the mesh by changing a. Then, after determining the optimal a, mesh convergence can be achieved by simply increasing N. By having the option to optimize a independent of both $r_{\min}$ and N, one can reduce the number of elements N required for a given accuracy, thus speeding up the calculation.

Exponential meshes in common use are special cases of the above more general one. For example the first and second meshes in [20] are given by

$$r_i = r_{\min} \left(\frac{r_{\max}}{r_{\min}} \right)^{(i-1)/N}. \tag{93}$$

Here, the meaning of i, N, $r_{\min}$, and $r_{\max}$ is the same as in (89). This form is a special case of (89) with $a = (r_{\max}/r_{\min})^{\frac{N-1}{N}}$. As such, the mesh is determined by three parameters $r_{\min}$, $r_{\max}$, and N, and the mesh gradation a depends on N and the fraction $r_{\max}/r_{\min}$. Note that this mesh does not allow $r_{\min} = 0$ (the mesh gradation would become infinite). For uranium, the first mesh has $N = 15788$, $r_{\min} = \frac{1}{160 \times 92}$, and $r_{\max} = 50$; from which it follows that $a = 7.353705 \times 10^5$. The second mesh has $N = 8000$, $r_{\min} = \frac{10^{-6}}{92}$, and $r_{\max} = \frac{800}{\sqrt{92}}$; from which it follows $a = 7.651530 \times 10^9$.

The third mesh in [20] is given by

$$r_i = A(e^{Bi} - 1). \tag{94}$$

The meaning of i is the same as in (89). The mesh is determined by three parameters A, B, and N. This is a special case of (89) with $r_{\min} = A(e^B - 1)$, $r_{\max} = A\left(e^{B(N+1)} - 1\right)$, and $a = e^{B(N-1)}$. For uranium, the values in [20] are $A = \frac{4.34}{92} \times 10^{-6}$, $B = 0.002304$, and $N = 9019$; from which it follows that $r_{\min} = 1.088140 \times 10^{-10}$, $r_{\max} = 50.031620$, and $a = 1.055702 \times 10^9$.

The fourth mesh in [20] is given by:

$$\rho_i = \log R_i, \tag{95}$$

	$r_{\min}$	$r_{\max}$	a	N
LDA	1.0e-07	50.0	2.7e+06	4866
RLDA	1.0e-08	50.0	6.2e+07	5268

Table 2
Optimal mesh parameters for 10^{-6} a.u. accuracy in total energy of uranium.

where ρ_i is a uniform mesh with N elements such that $R_1 = r_{\min}$ and $R_{N+1} = r_{\max}$. It follows that $\rho_i = \frac{i-1}{N} \log \frac{r_{\max}}{r_{\min}} + \log r_{\min}$. Then substituting into (95) and simplifying, the expression (93) is obtained. As such, the fourth mesh is equivalent to the first. For uranium, the values in [20] are $N = 2837$, $r_{\min} = \frac{10^{-6}}{92}$, and $r_{\max} = 50$; from which it follows that $a = 4.564065 \times 10^9$.

To summarize, the parameters of the four meshes for uranium in [20] are then as follows.

```
  | r_min              r_max          a             N
-------------------------------------------------------
1 | 6.79347826087e-05 50.0           7.353705e+05 15788
2 | 1.08695652174e-08 83.4057656228  7.651530e+09 8000
3 | 1.08814001246e-10 50.0316203306  1.055702e+09 9019
4 | 1.08695652174e-08 50.0           4.564065e+09 2837
```

In Section 4.3, we determine optimal parameters for LDA and RLDA calculations, as shown in Table 2. Here, the given $r_{\min}$, $r_{\max}$, and a can be used for all atoms, while the given N is sufficient for 10^{-6} a.u. accuracy in total energy for uranium; it can be increased for higher accuracy and decreased for lower atomic numbers Z to improve speed while retaining 10^{-6} accuracy, as we show in Section 4.3.

3.3 Shooting method for Schrödinger & Dirac eigenproblems

The required eigenfunctions are determined by the shooting method [17]: i.e., eigenvalues are guessed, radial integrations are performed, guesses are updated, and the process is repeated until convergence is achieved to the desired tolerance. For efficiency, we employ a combination of inward and outward integrations, bisection for robustness, and perturbation theory for efficiency once the solution is sufficiently close to convergence.

The outward integration starts at $r_{\min}$ using the asymptotic from Section 2 with $r = r_{\min}$, then RK4 is used for the first four steps, then Adams for the rest. For the inward integration, a starting point r_m is determined such that $e^{-\lambda r_m}$ is on the order of machine epsilon (e.g., $\sim 10^{-16}$ in double precision), with λ determined from the large-r asymptotic for the Schrödinger or Dirac

equation, as appropriate (Section 2). Then $e^{-\lambda r_m}$ is used for the last four points up to r_m and inward Adams is used for the rest.

The outward integration is performed up to the classical turning point r_{ctp}, defined by $V(r_{\text{ctp}}) = E$. Bisection is used to converge the energy to the point that the associated radial solution has the correct number of nodes $(n-l-1)$. After the correct number nodes is obtained, two approaches are considered to complete the eigenfunction computation.

The first approach is bisection: the outward integration is continued from r_{ctp} to the rest of the domain and the total number of nodes is counted. If the number is strictly greater than $n - l - 1$, then the energy E is above the eigenvalue, otherwise it is below the eigenvalue. Bisection is used to refine the eigenvalue to specified accuracy.

The second approach uses a perturbation correction for the energy, using both inward and outward integrations. It typically converges an order of magnitude faster than outward-only bisection once the correct number of nodes is obtained. For the Schrödinger equation, the following correction is used [23]:

$$E_2 \approx E_1 + \frac{P(r_{\text{ctp}})(Q(r_{\text{ctp}}^-) - Q(r_{\text{ctp}}^+))}{2\int_0^\infty P^2(r)\ \mathrm{d}r}, \tag{96}$$

where E_1 is the energy used to calculate $P(r)$ and $Q(r)$. The inward integration is multiplied by a constant so that it matches (in value) the outward integration at the classical turning point r_{ctp}. This leaves a jump in the derivative of the outward integration $Q(r_{\text{ctp}}^-)$ and inward integration $Q(r_{\text{ctp}}^+)$. E_2 is the new energy for the next iteration. Usually around five iterations are sufficient to achieve 10^{-13} accuracy in energy.

For Dirac equation, the following correction is used [23]:

$$E_2 \approx E_1 + c\frac{P(r_{\text{ctp}})(Q(r_{\text{ctp}}^-) - Q(r_{\text{ctp}}^+))}{\int_0^\infty P^2(r) + Q^2(r)\ \mathrm{d}r}. \tag{97}$$

After the correct number of nodes is determined, the perturbation correction is tried first. If it fails to converge (as can occur, e.g., for a too-confined domain), we fall back to outward-only bisection for robustness. For positive energies, the perturbation correction is inapplicable and outward-only bisection is used exclusively. Physically, the outward-only bisection method solves the atom in an infinite potential well of the size of the domain while the inward-outward perturbation method solves an atom in an infinite domain (by virtue of the asymptotic inward integration). As such, for large $r_{\max}$, the two methods converge to the same value, but for small $r_{\max}$ the eigenvalues can differ between methods. (An $r_{\max}$ study is needed to determine sufficient $r_{\max}$, as we show in Section 4).

All normalization and other integrals are calculated on $[r_{\min}, r_{\max}]$, avoiding the Coulomb singularity at $r = 0$. Hence, convergence with respect to $r_{\min}$ (typically $\sim 10^{-8}$ a.u.) must be checked, as we show in Section 4.

3.4 Outward Poisson integration

Since asymptotics are known at both ends of the domain (Section 2.3), it is possible to integrate the Poisson equation either inward or outward. We employ outward integration here in order to more accurately resolve rapid variations in core region. This better resolves the most tightly bound states (e.g., $1s$ and $2s$), in particular.

Since charge is omitted around the Coulomb singularity at $r = 0$ ($0 < r < r_{\min}$), we take as initial conditions, consistent with Eqs. (42) and (43):

$$V_H(r_{\min}) = 4\pi \int_{r_{\min}}^{r_{\max}} r n(r)\, \mathrm{d}r, \tag{98}$$

$$V_H'(r_{\min}) = 0. \tag{99}$$

Then RK4 is used for the first four points, after which the Adams method is used with predictor-corrector for the rest. Here again, convergence with respect to $r_{\min}$ must be checked, as we show in Section 4.

Having a precise Poisson solver is crucial to resolve all Kohn–Sham states accurately. With this outward solver, Kohn–Sham eigenvalues are typically an order of magnitude more precise than the total energy, with the most pronounced effect on the more tightly bound states. This is in contrast to other solvers [20] which typically resolve eigenvalues less accurately than total energies.

4 Results

4.1 Analytic test case: $V = -Z/r$

To verify the accuracy of the solver and establish convergence indicators, the Schrödinger and Dirac equations are solved for potential $V = -Z/r$ with $Z = 92$, for which analytic results are available. $r_{\min}$, $r_{\max}$, and N convergence studies are run for all eigenvalues with $n \leq 7$. In the resulting plots, $E - E_{\text{prev}}$ gives the change in energy with change of parameter being studied: e.g., as $r_{\min}$ is decreased toward convergence, $r_{\min} = 10^{-4}, 10^{-5}, \ldots, 10^{-14}$, $E - E_{\text{prev}}$ at $r_{\min} = 10^{-7}$ is the difference of computed energies at $r_{\min} = 10^{-7}$ and

n	l	dftatom	exact	diff
1	0	-4232.00000000001	-4232.00000000000	9.09e-12
2	0	-1058.00000000001	-1058.00000000000	7.28e-12
2	1	-1058.00000000000	-1058.00000000000	9.09e-13
3	0	-470.222222222232	-470.222222222222	9.55e-12
3	1	-470.222222222224	-470.222222222222	2.22e-12
3	2	-470.222222222224	-470.222222222222	2.22e-12
4	0	-264.500000000013	-264.500000000000	1.33e-11
4	1	-264.500000000005	-264.500000000000	5.00e-12
4	2	-264.500000000005	-264.500000000000	5.00e-12
4	3	-264.499999999997	-264.500000000000	3.18e-12
5	0	-169.280000000016	-169.280000000000	1.61e-11
5	1	-169.280000000011	-169.280000000000	1.08e-11
5	2	-169.280000000006	-169.280000000000	5.57e-12
5	3	-169.280000000006	-169.280000000000	5.57e-12
5	4	-169.280000000000	-169.280000000000	3.13e-13
6	0	-117.555555555579	-117.555555555556	2.34e-11
6	1	-117.555555555579	-117.555555555556	2.34e-11
6	2	-117.555555555572	-117.555555555556	1.61e-11
6	3	-117.555555555564	-117.555555555556	8.84e-12
6	4	-117.555555555557	-117.555555555556	1.55e-12
6	5	-117.555555555557	-117.555555555556	1.55e-12
7	0	-86.3673469388100	-86.3673469387755	3.44e-11
7	1	-86.3673469388046	-86.3673469387755	2.91e-11
7	2	-86.3673469387993	-86.3673469387755	2.38e-11
7	3	-86.3673469387886	-86.3673469387755	1.31e-11
7	4	-86.3673469387832	-86.3673469387755	7.73e-12
7	5	-86.3673469387779	-86.3673469387755	2.36e-12
7	6	-86.3673469387779	-86.3673469387755	2.36e-12

Table 3
Computed and exact Schrödinger eigenvalues for $V = -\frac{Z}{r}$.

$r_{\min} = 10^{-6}$. $E - E_{\text{conv}}$ is the difference of the computed energy from the fully converged value: e.g., $E - E_{\text{conv}}$ at $r_{\min} = 10^{-7}$ is the difference of energy at $r_{\min} = 10^{-7}$ from the fully converged value at $r_{\min}$ sufficiently small that reducing it further does not reduce the error further (due to finite precision).

For the Schrödinger equation, the $r_{\min}$ convergence study was run with $a = 10^9$, $r_{\max} = 50$, and $N = 50000$. From the resulting plot (Fig. 1a), we see that $r_{\min} = 10^{-7}$ is a converged value; decreasing $r_{\min}$ further does not reduce energy differences further. The $r_{\max}$ convergence study was run with $a = 2.7 \cdot 10^6$, $r_{\min} = 10^{-7}$, and $N = 50000$. From the resulting plot (Fig. 1b), we see that $r_{\max} = 3.5$ is a converged value. Finally, the N study was run with $a = 2.7 \cdot 10^6$, $r_{\min} = 10^{-7}$, and $r_{\max} = 50$. From the plot (Fig. 1c), it is determined that $N = 50000$ is a converged value.

From these results, it is seen that the fixed parameters for each convergence study were fully converged and the error indicator in each case was below 10^{-10} a.u. Table 3 compares the computed eigenvalues to exact values ($-\frac{Z^2}{2n^2}$) for this analytic test case and it is verified that the absolute error of the computed values is below 10^{-10}, as indicated by the convergence studies.

Of course, smaller N could be used to achieve the above accuracies using the converged $r_{\min}$ and $r_{\max}$ values indicated by the above studies, then optimizing

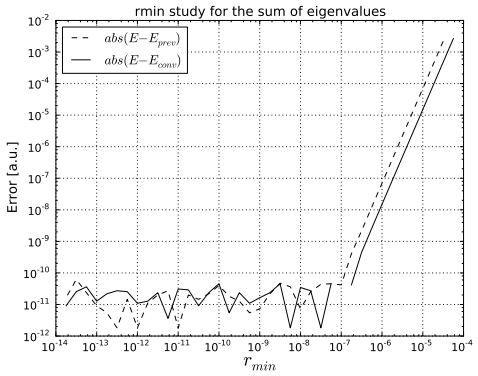

(a) r_{min} study

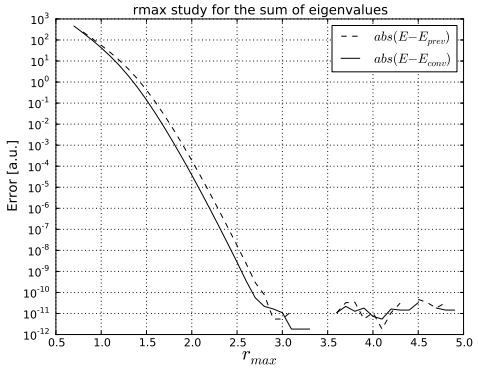

(b) r_{max} study

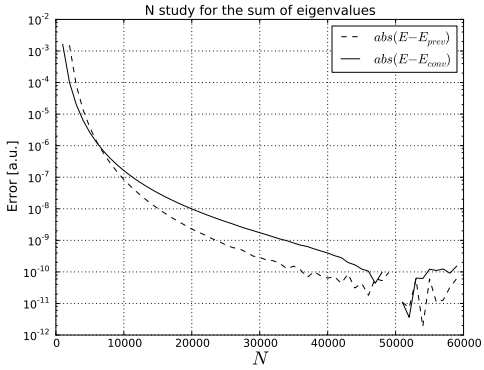

(c) N study

Fig. 1. Convergence studies for the sum of Schrödinger eigenvalues for $V = -Z/r$.

the mesh gradation a to minimize the required N. The purpose of the present analytic case study, however, is to verify the accuracy of the solver and establish the robustness of convergence indicators, $E - E_{\mathrm{prev}}$ and $E - E_{\mathrm{conv}}$. Optimal a and N are discussed in Section 4.3.

For the Dirac equation, the N study is first done for r_{min} larger than 10^{-11} and $N = 200000$ was obtained as a converged value ($a = 10^9$ was used so that

n	l	s	dftatom	exact	diff
1	0	1	-4861.19802311923	-4861.19802311937	1.41e-10
2	0	1	-1257.39589025788	-1257.39589025789	8.41e-12
2	1	1	-1089.61142091988	-1089.61142091987	1.59e-12
2	1	-1	-1257.39589025790	-1257.39589025789	1.75e-11
3	0	1	-539.093341793886	-539.093341793890	3.98e-12
3	1	1	-489.037087678200	-489.037087678200	1.14e-13
3	1	-1	-539.093341793896	-539.093341793890	5.68e-12
3	2	1	-476.261595161156	-476.261595161155	1.36e-12
3	2	-1	-489.037087678199	-489.037087678200	6.25e-13
4	0	1	-295.257844100398	-295.257844100397	1.42e-12
4	1	1	-274.407758840063	-274.407758840065	2.50e-12
4	1	-1	-295.257844100398	-295.257844100397	1.25e-12
4	2	1	-268.965877827131	-268.965877827130	9.66e-13
4	2	-1	-274.407758840063	-274.407758840065	1.88e-12
4	3	1	-266.389447187815	-266.389447187816	3.41e-13
4	3	-1	-268.965877827131	-268.965877827130	1.53e-12
5	0	1	-185.485191678549	-185.485191678552	3.01e-12
5	1	1	-174.944613583463	-174.944613583462	7.67e-13
5	1	-1	-185.485191678550	-185.485191678552	1.79e-12
5	2	1	-172.155252323734	-172.155252323737	2.67e-12
5	2	-1	-174.944613583463	-174.944613583462	6.54e-13
5	3	1	-170.828937049879	-170.828937049879	1.14e-13
5	3	-1	-172.155252323735	-172.155252323737	1.88e-12
5	4	1	-170.049934288550	-170.049934288552	2.36e-12
5	4	-1	-170.828937049878	-170.828937049879	1.19e-12
6	0	1	-127.093638842628	-127.093638842631	2.80e-12
6	1	1	-121.057538029547	-121.057538029549	1.44e-12
6	1	-1	-127.093638842628	-127.093638842631	2.26e-12
6	2	1	-119.445271987140	-119.445271987141	6.39e-13
6	2	-1	-121.057538029547	-121.057538029549	1.38e-12
6	3	1	-118.676410324351	-118.676410324351	1.28e-13
6	3	-1	-119.445271987140	-119.445271987141	3.13e-13
6	4	1	-118.224144624903	-118.224144624903	2.42e-13
6	4	-1	-118.676410324351	-118.676410324351	1.71e-13
6	5	1	-117.925825597294	-117.925825597293	1.34e-12
6	5	-1	-118.224144624903	-118.224144624903	4.41e-13
7	0	1	-92.4407876009401	-92.4407876009427	2.59e-12
7	1	1	-88.6717490520179	-88.6717490520168	1.05e-12
7	1	-1	-92.4407876009404	-92.4407876009427	2.30e-12
7	2	1	-87.6582876318895	-87.6582876318935	3.94e-12
7	2	-1	-88.6717490520179	-88.6717490520168	1.08e-12
7	3	1	-87.1739666719491	-87.1739666719477	1.35e-12
7	3	-1	-87.6582876318897	-87.6582876318935	3.77e-12
7	4	1	-86.8887663909435	-86.8887663909409	2.64e-12
7	4	-1	-87.1739666719491	-87.1739666719477	1.38e-12
7	5	1	-86.7005195728073	-86.7005195728088	1.55e-12
7	5	-1	-86.8887663909439	-86.8887663909409	3.06e-12
7	6	1	-86.5668751023587	-86.5668751023550	3.77e-12
7	6	-1	-86.7005195728072	-86.7005195728088	1.63e-12

Table 4
Computed and exact Dirac eigenvalues for $V = -\frac{Z}{r}$.

convergence was obtained for tractable N for all $r_{\min}$). The $r_{\min}$ study was then run and determined $r_{\min} = 10^{-8}$ as a converged value, giving accuracy better than $5 \cdot 10^{-10}$ a.u. $r_{\max} = 50$ was used and it was verified that it is a converged value. Table 4 shows a comparison of computed and exact Dirac

eigenvalues

$$E_{n\kappa} = \frac{c^2}{\sqrt{1 + \frac{(Z/c)^2}{(n-|\kappa|+\beta)^2}}} - c^2, \tag{100}$$

$$\beta = \sqrt{\kappa^2 - (Z/c)^2}, \tag{101}$$

for the Coulomb problem, and it is verified that the absolute error is below $5 \cdot 10^{-10}$ a.u., as indicated by the convergence studies. Note: all numerical and analytic calculations in this paper use the 1986 CODATA [30] recommended value $c = 137.0359895$ a.u., the same value as in NIST benchmarks [20].

4.2 Nonsingular test case: $V = \frac{1}{2}\omega^2 r^2$

Table 5 shows computed Schrödinger eigenvalues for the harmonic oscillator potential $V(r) = \frac{1}{2}\omega^2 r^2$ with $\omega = 1$ compared to exact values

$$E_{nl} = \omega\left(2n - l - \frac{1}{2}\right). \tag{102}$$

Asymptotics (10), (11) are used for outward integration, with perturbation correction turned off due to positive energies. It is seen that $r_{\min} = 10^{-7}$ a.u., $r_{\max} = 10$ a.u., $a = 10$ and $N = 5000$ are sufficient to obtain eigenvalues accurate to $< 10^{-8}$ a.u.

Table 6 shows Dirac eigenvalues for the harmonic oscillator potential $V(r) = \frac{1}{2}\omega^2 r^2$ with $\omega = 1$. Asymptotics (23), (24) and (25), (26) are used for outward integration, with perturbation correction again turned off due to positive energies. Lacking analytic results for comparison, we compared instead to independent high-order finite-element based calculations [31] which require no assumptions of asymptotic forms or determination of sufficiently small $r_{\min} > 0$. For $r_{\min} = 10^{-8}$ a.u., $r_{\max} = 10$ a.u., $a = 80$, and $N = 5000$, we find agreement of all eigenvalues to $< 10^{-8}$ a.u., with values very near to the corresponding Schrödinger results due to the relative weakness of the potential, in stark contrast to the singular Coulombic case. Note that, unlike the case of a singular potential, the number of nodes for $\kappa > 0$ is only $n - l$, whereas the number of nodes for $\kappa < 0$ remains $n - l - 1$, as in the singular case.

4.3 Uranium

We now consider full, self-consistent nonrelativistic (LDA) and relativistic (RLDA) Kohn–Sham calculations of uranium: a stringent test case, as numer-

n	l	dftatom	exact	diff
1	0	1.500000000168	1.500000000000	1.68E-10
2	0	3.500000000587	3.500000000000	5.87E-10
2	1	2.499999999999	2.500000000000	8.53E-13
3	0	5.500000001140	5.500000000000	1.14E-09
3	1	4.499999999993	4.500000000000	7.22E-12
3	2	3.499999999999	3.500000000000	1.19E-12
4	0	7.500000001777	7.500000000000	1.78E-09
4	1	6.499999999968	6.500000000000	3.18E-11
4	2	5.499999999990	5.500000000000	1.04E-11
4	3	4.499999999998	4.500000000000	1.53E-12
5	0	9.500000002451	9.500000000000	2.45E-09
5	1	8.499999999900	8.500000000000	1.00E-10
5	2	7.499999999955	7.500000000000	4.52E-11
5	3	6.499999999986	6.500000000000	1.42E-11
5	4	5.499999999998	5.500000000000	2.44E-12
6	0	11.500000003104	11.500000000000	3.10E-09
6	1	10.499999999751	10.500000000000	2.49E-10
6	2	9.499999999864	9.500000000000	1.36E-10
6	3	8.499999999940	8.500000000000	6.03E-11
6	4	7.499999999982	7.500000000000	1.85E-11
6	5	6.499999999997	6.500000000000	2.79E-12
7	0	13.500000003665	13.500000000000	3.66E-09
7	1	12.499999999466	12.500000000000	5.34E-10
7	2	11.499999999672	11.500000000000	3.28E-10
7	3	10.499999999824	10.500000000000	1.76E-10
7	4	9.499999999923	9.500000000000	7.66E-11
7	5	8.499999999977	8.500000000000	2.34E-11
7	6	7.499999999996	7.500000000000	3.69E-12

Table 5
Computed and exact Schrödinger eigenvalues for $V = \frac{1}{2}r^2$.

n	l	s	dftatom
1	0	0	1.49999501
2	0	0	3.49989517
2	1	0	2.49997504
2	1	1	2.49993510
3	0	0	5.49971548
3	1	0	4.49983527
3	1	1	4.49979534
3	2	0	3.49994176
3	2	1	3.49987520
4	0	0	7.49945594
4	1	0	6.49961565
4	1	1	6.49957572
4	2	0	5.49976206
4	2	1	5.49969551
4	3	0	4.49989517
4	3	1	4.49980199
5	0	0	9.49911657
5	1	0	8.49931620
5	1	1	8.49927627
5	2	0	7.49950252
5	2	1	7.49943598
5	3	0	6.49967554
5	3	1	6.49958238
5	4	0	5.49983526
5	4	1	5.49971547
6	0	0	11.49869739
6	1	0	10.49893692
6	1	1	10.49889699
6	2	0	9.49916315
6	2	1	9.49909661
6	3	0	8.49937608
6	3	1	8.49928292
6	4	0	7.49957572
6	4	1	7.49945594
6	5	0	6.49976205
6	5	1	6.49961565
7	0	0	13.49819839
7	1	0	12.49847782
7	1	1	12.49843790
7	2	0	11.49874396
7	2	1	11.49867742
7	3	0	10.49899680
7	3	1	10.49890364
7	4	0	9.49923634
7	4	1	9.49911657
7	5	0	8.49946258
7	5	1	8.49931619
7	6	0	7.49967553
7	6	1	7.49950251

Table 6
Computed Dirac eigenvalues for $V = \frac{1}{2}r^2$.

ous eigenstates are required, with tightly bound, highly oscillatory s states, spanning energies from ~ -0.1 to $\sim -40,000$ a.u.

We first determine sufficiently large $r_{\max}$ that the associated error (due to confining wavefunctions and potentials) is below the level of other sources in the calculation. We start by setting $r_{\min}$, $r_{\max}$, a, and N to typical values consistent with previous findings [20]. We then increase N to converge to the limit of finite precision. Then, increasing $r_{\max}$ in LDA (Figs. 2b and 2c) and RLDA (Figs. 3b and 3c) calculations (with perturbation correction turned off), considering both eigenvalues and total energy, shows that $r_{\max} = 50$ a.u. is a well converged value for both LDA and RLDA, consistent with previous findings [20].

The aim of the next N study is then to find N (and a) such that the total energy is converged for broad range of $r_{\min}$, so that such N can be used for the $r_{\min}$ study. In theory, by simply increasing N, the total energy must eventually converge, but for small a (low concentration of grid points around the origin), the required N might be very high. There is some coupling of $r_{\min}$ and a due to closer approach to the singularity at $r = 0$ for smaller $r_{\min}$: smaller $r_{\min}$ requires somewhat larger a for a given N and accuracy. It was found that using $a = 10^9$, full convergence is achieved for all $r_{\min} > 10^{-14}$ with $N = 50000$.

The initial point $r_{\min} > 0$ determines the accuracy of the asymptotics used to start the radial integrations, which are exact only in the limit $r \to 0$. The goal of the $r_{\min}$ study is to find fully converged $r_{\min}$ such that the associated error is at the limit of finite precision; so that decreasing further does not improve results. To do so, the fully converged a and N are taken from the initial N study, then converged total energies are calculated for all $r_{\min}$ from 10^{-14} to 10^{-5}.

Fig. 2a shows the $r_{\min}$ study for the LDA calculation. As can be seen, the total energy is converged for $r_{\min} = 10^{-7}$ and decreasing $r_{\min}$ further, the error indicators remain below the $5 \cdot 10^{-9}$ level. Choosing $r_{\min}$ smaller than 10^{-7} does not increase accuracy further. In general, choosing $r_{\min}$ as large as possible avoids the need for excessive grid points to resolve rapidly varying potentials, densities, and wavefunctions in the vicinity of the Coulomb singularity at $r = 0$. As such, $r_{\min} = 10^{-7}$ is used, as it gives sufficiently accurate asymptotics such that the associated errors are reduced to the limits of finite precision (which eliminates $r_{\min}$ from consideration when choosing other parameters), is consistent with values adopted previously [20], and is not so small as to require excessive grid points around the origin.

Fig. 3a shows the $r_{\min}$ study for the RLDA calculation. Using the same procedure as for the LDA calculation, $r_{\min} = 10^{-8}$ was chosen.

Now the optimal mesh for 10^{-6} a.u. accuracy in total energy is found by

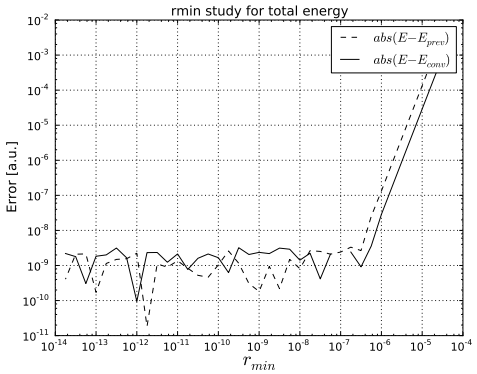

(a) $r_{\min}$ study total energy

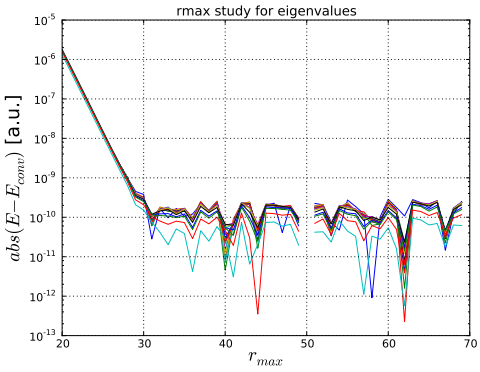

(b) $r_{\max}$ study eigenvalues

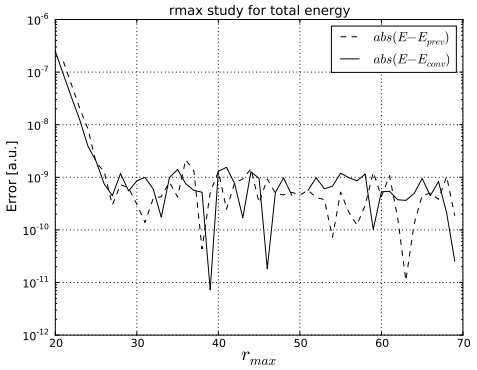

(c) $r_{\max}$ study total energy

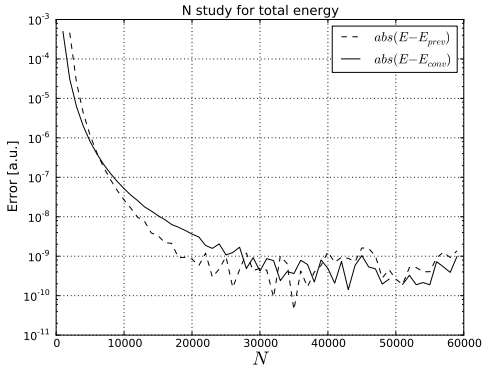

(d) N study total energy

Fig. 2. LDA (Schrödinger) DFT convergence studies for U.

setting $r_{\min}$ and $r_{\max}$ to converged values and varying the mesh gradation a to minimize the number of elements N required to achieve the specified accuracy. Proceeding in this way, we find optimal mesh parameters as in Table 2 for 10^{-6} a.u. accuracy in the total energy of uranium.

Having determined converged $r_{\min}$, $r_{\max}$, and optimized a (Table 2), we take N to convergence (Fig. 2d) to find converged total energy

$$E_{tot} = -25658.41788885\,\text{a.u.} \tag{103}$$

and orbital energies (Table 7) with error $< 10^{-8}$ a.u. for the LDA calculation.

Proceeding similarly for the RLDA calculation, we take N to convergence (Fig. 3d) to find converged total energy

$$E_{tot} = -28001.13232548\,\text{a.u.} \tag{104}$$

and orbital energies (Table 8) with error $< 10^{-8}$ a.u. for the RLDA calculation also.

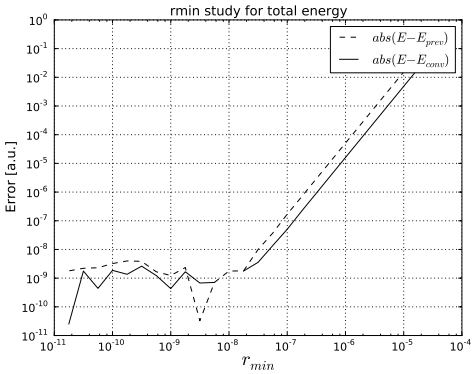

(a) r_{min} study total energy

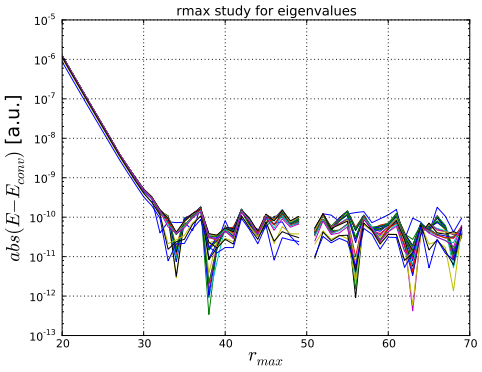

(b) r_{max} study eigenvalues

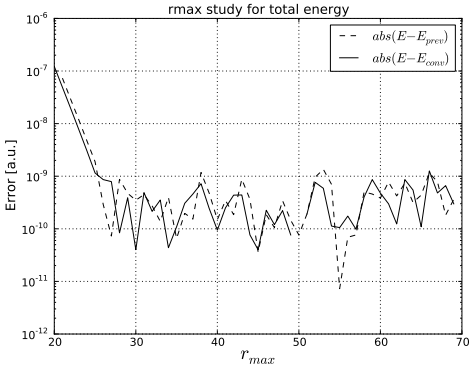

(c) r_{max} study total energy

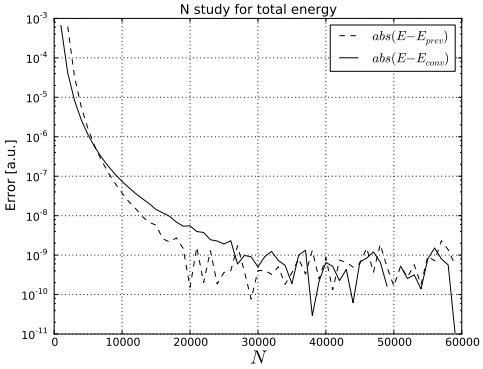

(d) N study total energy

Fig. 3. RLDA (Dirac) DFT convergence studies for U.

state	eigenvalue [a.u.]
1s	-3689.35513984
2s	-639.77872809
2p	-619.10855018
3s	-161.11807321
3p	-150.97898016
3d	-131.97735828
4s	-40.52808425
4p	-35.85332083
4d	-27.12321230
4f	-15.02746007
5s	-8.82408940
5p	-7.01809220
5d	-3.86617513
5f	-0.36654335
6s	-1.32597632
6p	-0.82253797
6d	-0.14319018
7s	-0.13094786

Table 7
Computed LDA eigenvalues for uranium (10^{-8} a.u. accurate).

state	eigenvalue [a.u.]
$1s_{1/2}$	-4223.41902045
$2s_{1/2}$	-789.48978233
$2p_{3/2}$	-761.37447597
$2p_{1/2}$	-622.84809456
$3s_{1/2}$	-199.42980564
$3p_{3/2}$	-186.66371312
$3p_{1/2}$	-154.70102667
$3d_{5/2}$	-134.54118029
$3d_{3/2}$	-128.01665738
$4s_{1/2}$	-50.78894806
$4p_{3/2}$	-45.03717129
$4p_{1/2}$	-36.68861049
$4d_{5/2}$	-27.52930624
$4d_{3/2}$	-25.98542891
$4f_{7/2}$	-13.88951423
$4f_{5/2}$	-13.48546969
$5s_{1/2}$	-11.29558710
$5p_{3/2}$	-9.05796425
$5p_{1/2}$	-7.06929564
$5d_{5/2}$	-3.79741623
$5d_{3/2}$	-3.50121718
$5f_{7/2}$	-0.14678839
$5f_{5/2}$	-0.11604717
$6s_{1/2}$	-1.74803995
$6p_{3/2}$	-1.10111900
$6p_{1/2}$	-0.77578418
$6d_{5/2}$	-0.10304082
$6d_{3/2}$	-0.08480202
$7s_{1/2}$	-0.16094728

Table 8
Computed RLDA eigenvalues for uranium (10^{-8} a.u. accurate).

4.3.1 Optimal N

In the previous section, for converged $r_{\min}$, $r_{\max}$, and optimized a (Table 2), sufficient N was determined to achieve 10^{-6} accuracy in total energies for uranium. In this section, we determine sufficient N for a series of accuracies, from 10^{-3} to 10^{-8} a.u., for all elements $Z = 1 - 92$.

Fig. 4a shows the required N for LDA (Schrödinger) and Fig. 4b for RLDA (Dirac) Kohn–Sham equations.

For simplicity, we use the same converged $r_{\min}$, $r_{\max}$, and optimized a (Table 2) for all atoms and just vary N for each atom to find a sufficient value for the specified accuracy.

The N shown in Figs. 4a and 4b is mainly for use as a starting point. Sufficient N will vary somewhat with the choice of exchange-correlation, and very much so with the choice of $r_{\min}$, $r_{\max}$, and a. If any of these are changed, as may be desired to find more optimal values for different atoms and/or accuracy requirements, a new N study will be required to determine sufficient N. If, however, the converged $r_{\min}$, $r_{\max}$, and a from Table 2 are used, then convergence can be attained for any atom to the limits of machine precision by

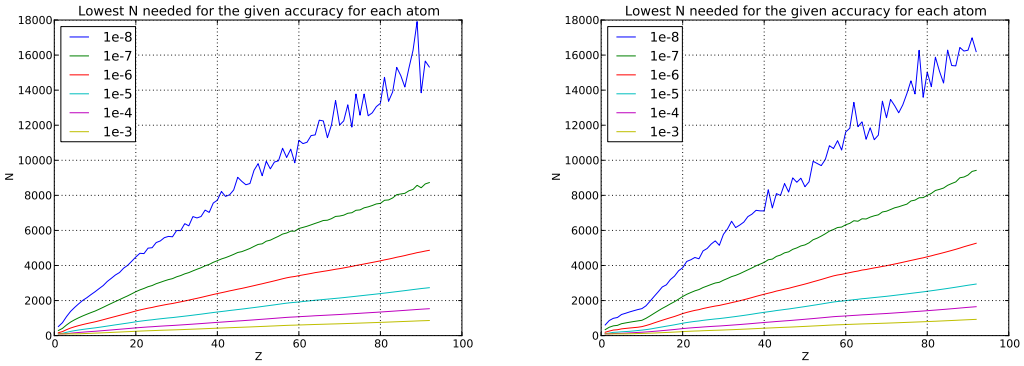

(a) Schrödinger (LDA) (b) Dirac (RLDA)

Fig. 4. Accuracy graph for LDA and RLDA DFT calculations.

simply increasing N.

By setting $N = 50000$ with converged $r_{\min}$, $r_{\max}$, and a from Table 2, fully converged total energies and Kohn–Sham eigenvalues are obtained, and used to compute errors for Figs. 4a and 4b.

4.3.2 Comparison to current benchmarks

Using the meshes from Table 2 with converged $N = 50000$, the computed Kohn–Sham total energies and eigenvalues were compared with current benchmark values [20,21] for all atoms $Z = 1 - 92$ for LDA (Schrödinger) and RLDA (Dirac) Kohn–Sham calculations. It was found that the computed total energies were all within $5.29 \cdot 10^{-7}$ of benchmark values for LDA and within $5.31 \cdot 10^{-7}$ for RLDA; and that the computed eigenvalues were all within 1.24×10^{-6} of benchmark values for LDA and within 1.37×10^{-6} for RLDA.

Reference [20] claims 10^{-6} a.u. absolute accuracy for Kohn–Sham total energies and finds maximum deviations among different codes of $2 \cdot 10^{-6}$ for associated eigenvalues. Our results, converged to $< 10^{-8}$ a.u., verify that the total energies reported in [20] indeed have absolute accuracy 10^{-6} a.u. or better; and furthermore, that the eigenvalues in [20] in fact have *absolute* accuracy $2 \cdot 10^{-6}$ a.u. or better.

5 Summary and conclusions

We have presented a robust and general solver for the solution of the radial Schrödinger, Dirac, and Kohn–Sham equations of density functional theory; and provided a modular, portable, and efficient Fortran 95 implementation,

`dftatom`, along with interfaces to other languages and full suite of examples and tests. The solver brings together ideas from many different codes developed over the decades, and some new ideas such as outward Poisson integration for increased accuracy in the core region and perturbation with fallback to bisection for speed and robustness. The solver can accommodate any potential, whether singular Coulombic or finite, and any mesh, whether linear, exponential, or otherwise. We have demonstrated the flexibility and accuracy of the associated code with solutions of Schrödinger and Dirac equations for Coulombic and harmonic oscillator potentials; and solutions of Kohn–Sham and Dirac–Kohn–Sham equations for the challenging case of uranium, obtaining energies accurate to 10^{-8} a.u., thus verifying and refining by two orders of magnitude current benchmarks [20]. We have shown detailed convergence studies in each case, providing mesh parameters to facilitate straightforward convergence to any desired accuracy by simply increasing the number of mesh points.

At all points in the design of the associated code, we have tried to emphasize simplicity and modularity so that the routines provided can be straightforwardly employed for a range of applications purposes, while retaining high efficiency. We have made the code available as open source to facilitate distribution, modification, and use as needed. We expect the present solvers will be of benefit to a range of larger-scale electronic structure methods which rely on atomic structure calculations and/or radial integrations more generally as key components.

6 Acknowledgements

We would like to thank Don Hamann and Mark Stiles for discussing and sharing their codes with us, as well as Eric Shirley for pointing us to other codes. We thank Charlotte Froese Fischer and Zbigniew Romanowski for helpful discussions and Peter Winkler for a critical reading of the manuscript.

This work performed, in part, under the auspices of the U.S. Department of Energy by Lawrence Livermore National Laboratory under Contract DE-AC52-07NA27344. This research was partly supported by the LC06040 research center project and GACR 101/09/1630 of the Czech Science Foundation.

References

[1] Richard M. Martin. *Electronic Structure: Basic Theory and Practical Methods*. Cambridge University Press, 2005.

[2] B. Wilson, V. Sonnad, P. Sterne, and W. Isaacs. PURGATORIO — a new implementation of the INFERNO algorithm. *J. Quant. Spectrosc. Radiat. Transf.*, 99(1-3):658–679, MAY-JUN 2006.

[3] W. H. Butler, P. H Dederichs, A. Gonis, and R. L. Weaver. *Application of Multiple Scattering Theory to Materials Science*. Materials Research Society, Pittsburg, Penn., 1992.

[4] H. L. Skriver. *The LMTO Method*. Springer, Berlin, 1984.

[5] D. J. Singh and L. Nordstrom. *Planewaves, Pseudopotentials, and the LAPW Method*. Springer, New York, 2nd edition, 2006.

[6] Emilio Artacho, E. Anglada, O. Dieguez, J. D. Gale, A. Garcia, J. Junquera, R. M. Martin, P. Ordejon, J. M. Pruneda, D. Sanchez-Portal, and J. M. Soler. The SIESTA method; developments and applicability. *J. Phys.: Cond. Matter*, 20(6), 2008. 2nd Workshop on Theory Meets Industry, Erwin Schrodinger Inst, Vienna, Austria, Jun 12-14, 2007.

[7] P. E. Blöchl. Projector augmented-wave method. *Phys. Rev. B*, 50(24):17953–17979, 1994.

[8] M. Marsman and G. Kresse. Relaxed core projector-augmented-wave method. *J. Chem. Phys.*, 125(10), SEP 14 2006.

[9] J. Vackář and A. Šimůnek. Adaptability and accuracy of all-electron pseudopotentials. *Phys. Rev. B*, 67(12712), 2003.

[10] J. P. Desclaux, D. F. Mayers, and F. O'Brien. Relativistic atomic wave functions. *J. Phys. B: At. Mol. Phys.*, 4:631–642, 1971.

[11] D. R. Hamann. Generalized norm-conserving pseudopotentials. *Phys. Rev. B*, 40:2980–2987, 1989.

[12] Per Jonsson, X He, Charlotte Froese-Fischer, and I. P. Grant. The grasp2k relativistic atomic structure package. *Comput. Phys. Commun.*, 177:597–622, 2007.

[13] A. R. Tackett, N. A. W. Holzwarth, and G. E. Matthews. A projector augmented wave (PAW) code for electronic structure calculations. *Comput. Phys. Commun.*, 135:348–376, 2001.

[14] Lin-Wang Wang et al. Petot. `https://hpcrd.lbl.gov/~linwang/PEtot/PEtot.html`, 2012.

[15] Kay Dewhurst et al. Elk. `http://elk.sourceforge.net/`, 2012.

[16] J. E. Pask and P. A. Sterne. Finite element methods in ab initio electronic structure calculations. *Model. Simul. Mater. Sci. Eng.*, 13(3):R71–R96, 2005.

[17] W. H. Press, S. A. Teukolsky, W. T. Vetterling, and B. P. Flannery. *Numerical Recipes: The Art of Scientific Computing*. Cambridge University Press, New York, 3 edition, 2007.

[18] Charlotte Froese Fischer and Oleg Zatsarinny. A B-spline Galerkin method for the Dirac equation. *Comput. Phys. Commun.*, 180(6):879–886, JUN 2009.

[19] I. P. Grant. B-spline methods for radial Dirac equations. *J. Phys. B: At. Mol. Opt. Phys.*, 42(5), MAR 14 2009.

[20] Svetlana Kotochigova, Zachary H. Levine, Eric L. Shirley, M. D. Stiles, and Charles W. Clark. Local-density-functional calculations of the energy of atoms. *Phys. Rev. A*, 55(1):191–199, 1997.

[21] National Institute of Standards and Technology. Atomic reference data for electornic structure calculations. `http://physics.nist.gov/PhysRefData/DFTdata/`, 1997.

[22] O. Čertík, J. E. Pask, and J. Vackář. dftatom. `http://sourceforge.net/projects/dftatom/`, 2012.

[23] Walter R. Johnson. Lectures on atomic physics. `http://nd.edu/~johnson/Publications/book.pdf`, 2006.

[24] Paul Strange. *Relativistic Quantum Mechanics*. Cambridge University Press, 1998.

[25] J. Zabloudil, R. Hammerling, L. Szunyogh, and P. Weinberger. *Electron Scattering in Solid Matter*. Springer-Verlag Berlin, 2005.

[26] I. P. Grant. The Dirac operator on a finite domain and the R-matrix method. *J. Phys. B: At. Mol. Opt. Phys.*, 41(5):1–9, March 2008.

[27] M. Oulne. Analytical solution of the Thomas-Fermi equation for atoms. *Int. Rev. Phys.*, 4(6):349–352, 2010.

[28] S. H. Vosko, L. Wilk, and M. Nusair. Accurate spin-dependent electron liquid correlation energies for local spin density calculations: a critical analysis. *Can. J. Phys.*, 58(1200), 1980.

[29] A. H. MacDonald and S. H. Vosko. A relativistic density functional formalism. *J. Phys. C: Solid St. Phys.*, 12(2977-2990), 1979.

[30] E. Richard Cohen and Barry N. Taylor. The 1986 adjustment of the fundamental physical constants. *Rev. Mod. Phys.*, 59(4):1121–1148, 1987.

[31] O. Čertík and J. E. Pask. High-order finite element method for atomic structure calculations. In preparation.